



Cross-Modality Supervised Prostate Segmentation on CBCT for Adaptive Radiotherapy

Balint Kovacs^{1,2,*}, Goran Stanic^{3,4,5*}, Fabian Weykamp^{4,6,7,8}, Florian Ebert², Dimitrios Bounias^{1,2}, Bouchra Tawk^{4,6,7,8}, Martin Niklas^{3,9}, Jakob Liermann^{7,8}, Oliver Jäkel^{3,4,7,8}, Klaus H. Maier-Hein^{1,8,10}, Ralf Floca^{1,4,†}, and Kristina Giske^{3,4,†}

¹ German Cancer Research Center (DKFZ) Heidelberg,

Division of Medical Image Computing (MIC), Heidelberg, Germany

² Medical Faculty Heidelberg, Heidelberg University, Heidelberg, Germany

³ DKFZ Heidelberg, Division of Medical Physics in Radiation Oncology, Germany

⁴ Heidelberg Institute of Radiation Oncology (HIRO), National Center for Radiation Research in Oncology (NCRO), Heidelberg, Germany

⁵ Faculty of Physics and Astronomy, University of Heidelberg, Heidelberg, Germany

⁶ DKFZ Heidelberg, Clinical Cooperation Unit Radiation Oncology, Germany.

⁷ Department of Radiation Oncology, Heidelberg Ion-Beam Therapy Center (HIT), Heidelberg University Hospital, Heidelberg, Germany

⁸ National Center for Tumor Diseases (NCT), Heidelberg, Germany

⁹ DKFZ Heidelberg, Division of Radiology, Germany

¹⁰ Pattern Analysis and Learning Group, Department of Radiation Oncology, Heidelberg University Hospital, Heidelberg, Germany
{balint.kovacs,goran.stanic}@dkfz-heidelberg.de

Abstract. Accurate organ segmentation is crucial for prostate cancer radiotherapy, but cone-beam computer tomography (CBCT) based models are hindered by low image quality and annotation scarcity. Existing approaches rely on deformable registration, which struggles with soft-tissue deformations, or direct CBCT training, which suffers from domain shifts and low-quality labels. We propose a domain adaptation framework that enables robust prostate segmentation on CBCT using cross-modality supervision from planning CT (pCT). A cycle-consistent generative adversarial network translates pCT into synthetic CBCT, enabling segmentation models to train on high-quality pCT-derived annotations while adapting to CBCT characteristics. Additionally, anatomy-aware augmentation enhances robustness to organ deformations across diverse patient anatomies. Using a multi-center dataset, our approach achieves segmentation accuracy comparable to pCT-trained models. By eliminating the need for manual CBCT annotations, our method enables practical AI-driven segmentation for adaptive radiotherapy.

Keywords: Adaptive radiotherapy · Semantic segmentation · Domain adaptation · Organ deformations.

* Equal contribution; each may list themselves as lead co-first author.

† Shared last authorship.

1 Introduction

Accurate organ delineation is crucial for prostate radiation therapy (RT), as continuous anatomical changes require frequent dose adaptations to precisely target the prostate while minimizing radiation exposure to surrounding healthy tissues [6,14]. Cone-beam computed tomography (CBCT) is widely used for treatment adaptation, but its low image quality and poor soft-tissue contrast make organ delineation time-consuming and error-prone [16,11]. Furthermore, soft tissue deformations occurring during the lengthy contouring process can render delineations outdated before treatment begins [20]. The lack of high-quality annotations and inherent imaging challenges hinder the adoption of AI-driven segmentation in clinical workflows.

Existing automated solutions fall short in addressing these challenges. Deformable image registration, which transfers segmentations from planning CT (pCT) to CBCT, is unreliable in cases of strong local soft-tissue deformations, as it requires regularization to avoid unrealistic warping [2,19]. Convolutional neural networks (CNNs), particularly nnU-Net [7], have demonstrated strong performance in medical image segmentation, but training a reliable model requires large, well-annotated datasets – an obstacle for CBCT due to the lack of high-quality ground truth (GT). Monte Carlo simulations can bridge the pCT and CBCT domains for CNN training [1], but they are complex, device-specific, and prone to modeling errors. Another approach involves using CycleGANs to generate synthetic CTs or MRIs from CBCTs to aid in automatic organ at risk contouring [5,3]. However, this method remains fundamentally limited as it attempts to generate high-quality or different-domain images from inherently low-detail input data.

In this work, we propose a **cross-modality supervised domain translation framework** for prostate segmentation in CBCT, addressing challenges of low image quality and annotation scarcity. Instead of enhancing CBCT quality, we generate synthetic CBCT (synCBCT) from pCT using a CycleGAN-based $pCT \mapsto CBCT$ translation. This allows us to train segmentation models on synCBCT while leveraging high-quality pCT-derived annotations. Additionally, **anatomy-aware augmentation** [9] enhances robustness to soft-tissue deformations, ensuring reliable segmentation in real-world clinical scenarios.

We are the first to introduce this cross-modality-supervised learning paradigm for CBCT segmentation, effectively bridging the domain gap without requiring manual CBCT annotations. By combining generative modeling with robust augmentation strategies, our method facilitates clinically viable AI-driven segmentation for adaptive radiotherapy, reducing annotation burden while improving treatment precision.

2 Methods

Our key innovation is providing high-quality, pCT-derived ground truth (GT) for training segmentation networks on CBCT, as outlined in Fig 1. To achieve this,

we use the $pCT \mapsto CBCT$ branch of a CycleGAN that degrades high-quality pCT images into synthetic CBCT. This fully learnable strategy avoids the pitfalls of simulation- and deformation-based methods. We then train the nnU-Net, a state-of-the-art medical segmentation network, using synCBCT images generated from pCT while transferring the original pCT segmentations as GT. This approach allows the network to leverage high-quality pCT annotations while operating in the CBCT domain. As a result, our method bridges the domain gap without compromising segmentation quality.

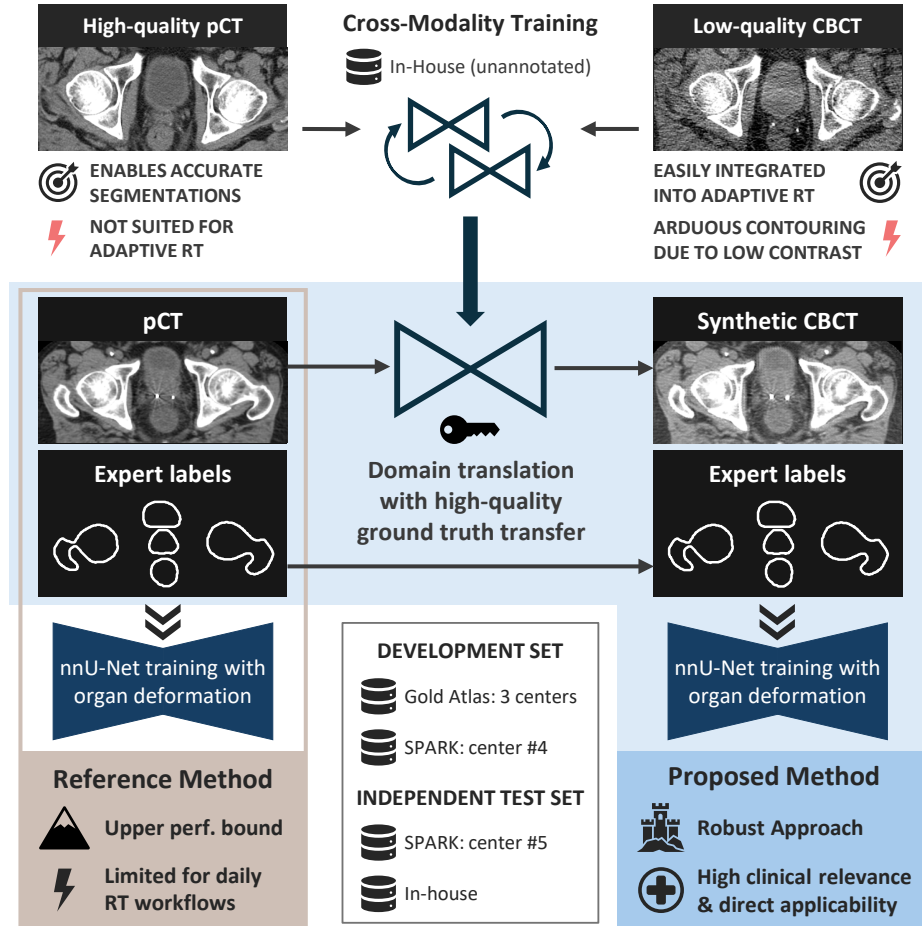


Fig. 1. Our proposed framework addressing annotation scarcity on low-quality CBCT images. By combining generative modeling with robust augmentation strategies, our method facilitates clinically viable AI-driven segmentation for adaptive radiotherapy.

2.1 Characteristics of Datasets

Our study includes 56 images from 6 institutes as detailed below. All images used in the study were resampled to an in-plane spacing of 0.875 mm and a slice thickness of 2.5 mm. TotalSegmentator [21] was used to extract the body contour and remove the imaging or treatment table. Organ contours included in the study were: femur, bladder, rectum, penile bulb, prostate, and seminal vesicles.

■ **SPARK & ■ Gold Atlas** – pCT images from two external open access datasets, SPARK [8] and Gold Atlas [13] were used. 2 out of 5 treatment centers (4+3 patients) from the SPARK dataset were included for the study with the criterion that prostate contours exist and are separated from the seminal vesicles. All 3 centers from the Gold Atlas dataset were represented by 19 (8+7+4) patients. Contours associated with the Gold Atlas were delineated on MRI, and the pCTs were deformably registered to the same MRIs, while the SPARK dataset contained organ structures that were contoured directly on the pCT. The distance between the prostate and penile bulb was measured to assess compliance with ESTRO guidelines, which specify a minimum separation of 1 cm between these structures. The mean prostate-penile bulb distance was 12.0 ± 4.8 cm, with 8 patients (42.1%) failing to meet the minimum separation requirement.

■ **Unannotated in-house pCT and CBCT** – 27 prostate cancer (PCa) patients treated with EthosTM (Varian - A Siemens Healthineers, Palo Alto, CA) at the DKFZ were chosen for the study. A pCT and three equally spaced fraction CBCT images from each patient were used for network training.

■ **Annotated in-house CBCT** – Three CBCTs from separate patients treated with EthosTM at the DKFZ were contoured by a medical student (F.E.) following ESTRO ACROP delineation guidelines [16], under a standard procedure developed with guidance from a senior radiation oncologist (F.W.) to ensure proper interpretation and application. The University Hospital Heidelberg ethics committee approved the study (S-511/2023), with informed consent from all patients.

2.2 Experimental Setting & Evaluation for Two Key Questions

1. Can CBCT with enhanced GT provide as much information for model training as high-quality pCT? – We train two segmentation models using the same pCT-contoured ground truth: one on pCT images and another on synCBCT images generated via the $pCT \mapsto CBCT$ branch of CycleGAN. This ensures that the only difference in training is the information content within the imaging domain. The model trained on pCT serves as an upper performance bound, while the model trained on low-quality CBCT with enhanced GT aims to match its performance. Additionally, we increase model robustness by simulating soft tissue deformations during model training [9] and we optimize its parameters on the pCT training. We use an independent test set from a single center in the ■ SPARK dataset for evaluation - original pCT images for the model trained on pCTs and synCBCT images for the model trained on synCBCTs.


2. Can our method achieve competitive performance on clinical data? We evaluate our segmentation models on three increasingly difficult cases with distinct properties from our independent ■ annotated in-house CBCT dataset.

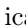
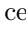

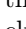
- Slim patient with moderate beam hardening artifacts
- Patient with prostate growth into the bladder
- Obese patient with severe beam hardening \Rightarrow barely visible organ contours

This dataset serves as a clinical validation and also helps determine whether training directly on CBCT is necessary or if pCT-trained models suffice.

Evaluation Metrics Quantitatively, we evaluated the CycleGAN network performance using structural similarity, mean squared error, and Jensen-Shannon divergence. In all cases, the generated images were closer to the target modality than to the input. Qualitatively, we visually inspected the generated images, confirming their anatomical fidelity and realism. To evaluate the segmentation model performance and assess label similarity and distance we used three metrics: volumetric overlap using the Sørensen–Dice coefficient (DICE) [4,18], fraction of deviation larger than 2 mm using surface DICE (sDICE) as defined in [12], and 95th percentile distance between two contours using Hausdorff distance (HD) in mm [15]. The metrics were calculated for three structures: prostate, rectum, and bladder. To ensure clinical relevance, we limited the evaluation to image slices within the typical extent of the prostate planning target volume in radiotherapy in the inferior and posterior directions (7-10 mm) [11]. Due to truncated rectum segmentations in our development dataset, we set the inferior limit to the maximum extent of the prostate contour. We also evaluate adherence to the ESTRO guidelines [16], particularly regarding the distance from the prostate to the penile bulb.

2.3 Model Training of the Proposed Strategy

Domain-translation Network Training – pCT and CBCT images from the  unannotated in-house dataset were split into a training set (22) and a test set (5). Three equally spaced fractions from each patient were used as a form of data augmentation. CT-values were clipped to [-1000, 2000] HU and normalized to [-1, 1] for training. A 3D generative neural network for unpaired image-to-image translation (3DCycleGAN) was used for synCBCT generation based on the original work [22]. A ResNet-based generator and a Markovian discriminator were used as the network backbone. Network was trained on randomly selected patches of size (256, 256, 32). Postprocessing steps included predicting overlapping patches, averaging the values in the overlapping regions, and renormalizing the images to [-1000, 2000] HU.

Segmentation Network Training – The 29 patients were stratified by medical center and available GT structures into a **training set** (4 from  SPARK center#4, 19 from  GOLD ATLAS all of the 3 centers) and a **test set** (3 from  SPARK center#5 and 3 from  annotated in-house). The test set included the prostate, bladder, rectum, and penile bulb, while the training set also included the femur and seminal vesicles. Images were global z-score normalized using nnU-Net preprocessing. 3D nnU-Net models were trained in 5-fold cross-validation (5fCV), adopting the anatomy-informed augmentation [9] to enhance robustness against organ deformations. Hyperparameters for the deformations

were optimized based on 5fCV results. In the final model, either rectum or bladder deformations were applied with a 7.5 % probability each, using a Gaussian kernel $\sigma = 8$ and deformation amplitude sampled uniformly in $C = [-75, 75]$. Postprocessing was done by the nnU-Net pipeline.


We make our code publicly available in the repositories <https://github.com/DKFZ-OpenMedPhys/3DcycleGAN> & [/MIC-DKFZ/anatomy_informed_DA](https://github.com/MIC-DKFZ/anatomy_informed_DA).

3 Results

The first part of our results aims to answer the first research question we posed in Section 2.2. Incorporating rectal and bladder deformations during model training shows improved or unchanged 5fCV segmentation performance, see Table 1. Models trained on pCT and synCBCT with enhanced GT perform comparably (see Table 2), even with slight HD improvements. Our method is just 0.01 below the upper bound in all DICE and sDICE metrics, except for prostate sDICE.

Table 1. Model training on pCT with and without simulating organ deformations

Training with organ deform.	Prostate			Rectum			Bladder		
	HD	sDICE	DICE	HD	sDICE	DICE	HD	sDICE	DICE
No	5.0	0.63	0.83	7.3	0.65	0.79	4.7	0.80	0.88
	± 1.2	± 0.12	± 0.06	± 2.8	± 0.15	± 0.08	± 3.5	± 0.10	± 0.06
Yes	5.0	0.64	0.83	6.9	0.66	0.79	4.6	0.81	0.89
	± 1.2	$\pm \mathbf{0.11}$	$\pm \mathbf{0.05}$	$\pm \mathbf{2.5}$	$\pm \mathbf{0.15}$	± 0.08	$\pm \mathbf{3.2}$	$\pm \mathbf{0.10}$	$\pm \mathbf{0.06}$

Table 2. Segmentation results and differences on the independent  SPARK center #5 between the pCT-trained model (upper bound) and the synCBCT-trained model with enhanced GT (proposed)

Training Modality	Prostate			Rectum			Bladder		
	HD	sDICE	DICE	HD	sDICE	DICE	HD	sDICE	DICE
pCT	4.2	0.63	0.84	3.3	0.90	0.89	4.2	0.83	0.89
(upper bound)	± 0.6	$\pm \mathbf{0.09}$	$\pm \mathbf{0.01}$	± 1.0	$\pm \mathbf{0.06}$	± 0.01	± 2.4	$\pm \mathbf{0.10}$	$\pm \mathbf{0.06}$
synCBCT	4.1	0.59	0.83	3.0	0.89	0.89	4.2	0.82	0.88
(proposed)	$\pm \mathbf{0.4}$	± 0.09	± 0.02	$\pm \mathbf{1.1}$	± 0.09	± 0.02	$\pm \mathbf{2.3}$	± 0.11	± 0.07
Difference	0.1	0.04	0.01	0.3	0.01	0.00	0.0	0.01	0.01


To address the clinical need and viability of our proposed method (second research question in Section 2.2), we compare the performance of models trained on synCBCT with enhanced ground truth against those trained on planning CT, on an  annotated in-house dataset. The synCBCT-trained models demonstrate significant improvements in prostate and rectum segmentation across all

Table 3. Segmentation results on the ■ annotated in-house dataset (CBCT) for the pCT-trained model and the synCBCT-trained model with enhanced GT (proposed)

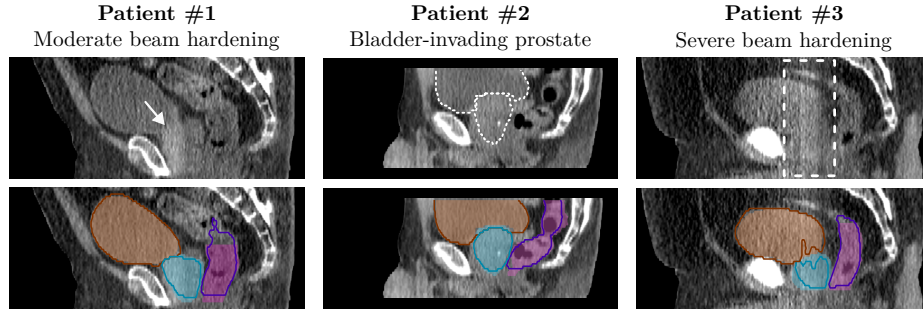
Training Modality	Prostate			Rectum			Bladder		
	HD	sDICE	DICE	HD	sDICE	DICE	HD	sDICE	DICE
pCT	8.8 ± 3.6	0.43 ± 0.23	0.75 ± 0.11	7.7 ± 6.4	0.76 ± 0.14	0.83 ± 0.05	2.8 ± 1.2	0.91 ± 0.06	0.94 ± 0.03
synCBCT (proposed)	7.2 ± 2.4	0.50 ± 0.23	0.78 ± 0.10	7.5 ± 4.3	0.79 ± 0.04	0.83 ± 0.01	4.4 ± 3.2	0.86 ± 0.04	0.87 ± 0.05

Table 4. Segmentation results of the ■ annotated in-house dataset case-by-case analysis for a synCBCT-trained model

In-house patient	Prostate			Rectum			Bladder		
	HD	sDICE	DICE	HD	sDICE	DICE	HD	sDICE	DICE
#1	6.6	0.62	0.83	12.5	0.75	0.83	2.5	0.91	0.93
#2	5.0	0.65	0.85	5.1	0.78	0.82	8.3	0.83	0.86
#3	9.8	0.23	0.66	5.0	0.83	0.85	2.5	0.85	0.83

evaluation metrics, while planning CT-trained models show superior bladder segmentation (Table 3). Observing the results on a case-by-case basis Table 4 shows variable results which will be further discussed in Section 4.

The prostate-penile bulb distance for the synCBCT-trained model was 10.0 ± 4.7 mm for the ■ SPARK center #5, while 10.0 ± 2.5 mm for the ■ annotated in-house dataset.

**Fig. 2.** Visualization of segmentation results for three patients from the annotated in-house dataset. The top row highlights case characteristics, while the bottom row shows predicted contours (lines) overlaid on the ground truth (shaded regions).

4 Discussion

The integration of AI-driven segmentation into adaptive radiotherapy workflows presents several technical challenges, particularly regarding the quality and avail-

ability of training data in CBCT imaging. While previous approaches have relied heavily on manual annotations of low-quality CBCT images, this work explores an alternative strategy using domain adaptation. The following discussion examines our findings through several key aspects: the impact of synthetic training data on segmentation accuracy, the role of organ deformation in model robustness, and the potential clinical implications of our framework.

Robust Performance Approaching the Upper Bound - Research question No. 1 – The segmentation model trained on synCBCT with enhanced GT achieved performance comparable to the model trained on high-quality pCT, showing either no difference or competitive results. This suggests that the model effectively extracted sufficient features to compensate for lower image quality. While pCT and CBCT share the fundamental physics of X-ray attenuation, they differ in their acquisition parameters, scatter contributions, and reconstruction methods. Both modalities present challenges in soft-tissue contrast compared to MRI, particularly in the pelvic region, though CBCT typically exhibits lower contrast-to-noise ratio and increased scatter artifacts compared to pCT [17,10]. The model’s ability to perform well despite these differences may be attributed to the high-quality labels used during training. Additionally, incorporating organ deformations due to bladder and rectal size variations improved segmentation.

Promising Clinical Feasibility Assessment - Research Question No. 2 The superior prostate segmentation performance of our model on the annotated in-house CBCT dataset suggests that models trained on target domain data may offer advantages for prostate segmentation compared to models trained on pCT. Although the cases were considered challenging, these findings should be considered early indicators rather than definitive conclusions given the limited sample size. Performance across OARs was mixed: rectum segmentation showed potential improvements, while bladder segmentation remained comparable to SPARK dataset results. Case-by-case analysis revealed that the model handled moderate beam hardening artifacts, and bladder-invading prostate growth well, but struggled with severe imaging artifacts. These findings align with expectations given the limited size of the development set, where such complex cases were likely underrepresented. The observed performance trends are promising, further motivating future research with expanded training data. In addition to segmentation accuracy, inference speed and integration into clinical workflows are critical for real-world adoption. During deployment, only the segmentation network operates on CBCTs, yielding inference times <30 s/CBCT on an NVIDIA RTX 2080 (<10.7 GB). This is substantially faster than approaches requiring sequential synthesis and segmentation, aligning well with the clinical demands of prostate RT where minimizing on-table latency is crucial to prevent anatomical changes that can quickly render images outdated.

Compliance with ESTRO ACROP guidelines – Segmentation models predicted prostate and penile bulb structures with distances that generally complied with the ESTRO ACROP guidelines for both the SPARK and in-house datasets, though some individual cases violated the minimum required distance. This suggests that the models learned the spatial correlation of structures to the extent

allowed by the training data. Therefore, training the models on fully ESTRO ACROP-compliant data is likely to yield compliance on the evaluation dataset.

5 Conclusion

This paper aims to facilitate clinically applicable AI-driven prostate and organ-at-risk segmentation for adaptive radiotherapy by overcoming the annotation burden on low-quality CBCT images, ultimately improving treatment precision. To achieve this, we proposed a domain adaptation framework that enables training on synthetic CBCT images using high-quality pCT-derived annotations while accounting for organ deformations by incorporating them into the training to enhance the robustness necessary in daily clinical practice. Our training strategy demonstrated promising results comparable to models trained on high-quality images and demonstrated the feasibility of clinically viable AI-driven segmentation for adaptive radiotherapy on a set of challenging clinical cases.

Acknowledgments. This study was partially funded by a Varian Research Grant from Varian, A Siemens Healthineers Company.

Disclosure of Interests. F.W. received speaker fees from AstraZeneca, Varian and Merck Sharp & Dohme and travel support for attending meetings from Varian and Micropos Medical.

References

1. Abbani, N., Baudier, T., Rit, S., Franco, F.d., Okoli, F., Jaouen, V., Tilquin, F., Barateau, A., Simon, A., de Crevoisier, R., et al.: Deep learning-based segmentation in prostate radiation therapy using Monte Carlo simulated cone-beam computed tomography. *Medical Physics* **49**(11), 6930–6944 (2022) [2](#)
2. Acosta, O., Dowling, J., Drean, G., Simon, A., De Crevoisier, R., Haignon, P.: Multi-atlas-based segmentation of pelvic structures from CT scans for planning in prostate cancer radiotherapy. In: *Abdomen and thoracic imaging: an engineering & clinical perspective*, pp. 623–656. Springer (2013) [2](#)
3. Dai, X., Lei, Y., Wynne, J., Janopaul-Naylor, J., Wang, T., Roper, J., Curran, W.J., Liu, T., Patel, P., Yang, X.: Synthetic CT-aided multiorgan segmentation for CBCT-guided adaptive pancreatic radiotherapy. *Medical physics* **48**(11), 7063–7073 (2021) [2](#)
4. Dice, L.R.: Measures of the amount of ecologic association between species. *Ecology* **26**(3), 297–302 (1945) [5](#)
5. Fu, Y., Lei, Y., Wang, T., Tian, S., Patel, P., Jani, A.B., Curran, W.J., Liu, T., Yang, X.: Pelvic multi-organ segmentation on cone-beam CT for prostate adaptive radiotherapy. *Medical physics* **47**(8), 3415–3422 (2020) [2](#)
6. Ghilezan, M., Yan, D., Martinez, A.: Adaptive radiation therapy for prostate cancer. In: *Seminars in radiation oncology*. vol. 20, pp. 130–137. Elsevier (2010) [2](#)
7. Isensee, F., Jaeger, P.F., Kohl, S.A.A., Petersen, J., Maier-Hein, K.H.: nnu-net: a self-configuring method for deep learning-based biomedical image segmentation. *Nature Methods* **18**(2), 203–211 (2021) [2](#)

8. Keall, P., Nguyen, D.T., O'Brien, R., Hewson, E., Ball, H., Poulsen, P., Booth, J., Greer, P., Hunter, P., Wilton, L., et al.: Real-time image guided ablative prostate cancer radiation therapy: results from the TROG 15.01 SPARK trial. *International Journal of Radiation Oncology* Biology* Physics* **107**(3), 530–538 (2020) [4](#)
9. Kovacs, B., Netzer, N., Baumgartner, M., Eith, C., Bounias, D., Meinzer, C., Jäger, P.F., Zhang, K.S., Floca, R., Schrader, A., et al.: Anatomy-informed data augmentation for enhanced prostate cancer detection. In: *International Conference on Medical Image Computing and Computer-Assisted Intervention*. pp. 531–540. Springer (2023) [2](#), [4](#), [5](#)
10. Lechuga, L., Weidlich, G.: Cone beam CT vs. fan beam CT: A comparison of image quality and dose delivered between two differing CT imaging modalities. *Cureus* **8**(9), e778 (9 2016) [8](#)
11. Li, G., Li, Y., Wang, J., Gao, X., Zhong, Q., He, L., Li, C., Liu, M., Liu, Y., Ma, M., et al.: Guidelines for radiotherapy of prostate cancer (2020 edition). *Precision Radiation Oncology* **5**(3), 160–182 (2021) [2](#), [5](#)
12. Nikolov, S., Blackwell, S., Zverovitch, A., Mendes, R., Livne, M., De Fauw, J., Ronneberger, O.: Clinically applicable segmentation of head and neck anatomy for radiotherapy: deep learning algorithm development and validation study. *Journal of Medical Internet Research* **23**(7), e26151 (2021) [5](#)
13. Nyholm, T., Svensson, S., Andersson, S., Jonsson, J., Sohlén, M., Gustafsson, C., Kjellén, E., Söderström, K., Albertsson, P., Blomqvist, L., et al.: MR and CT data with multiobserver delineations of organs in the pelvic area—part of the gold atlas project. *Medical physics* **45**(3), 1295–1300 (2018) [4](#)
14. Peng, C., Ahunbay, E., Chen, G., Anderson, S., Lawton, C., Li, X.A.: Characterizing interfraction variations and their dosimetric effects in prostate cancer radiotherapy. *International Journal of Radiation Oncology* Biology* Physics* **79**(3), 909–914 (2011) [2](#)
15. Rogers, C.A.: Hausdorff Measures. Cambridge University Press (1998) [5](#)
16. Salembier, C., Villeirs, G., De Bari, B., Hoskin, P., Pieters, B.R., Van Vulpen, M., Khoo, V., Henry, A., Bossi, A., De Meerleer, G., et al.: ESTRO ACROP consensus guideline on CT-and MRI-based target volume delineation for primary radiation therapy of localized prostate cancer. *Radiotherapy and Oncology* **127**(1), 49–61 (2018) [2](#), [4](#), [5](#)
17. Siewerdsen, J.H., Jaffray, D.A.: Cone-beam computed tomography with a flat-panel imager: magnitude and effects of x-ray scatter. *Medical Physics* **28**(2), 220–231 (2001) [8](#)
18. Sorensen, T.: A method of establishing groups of equal amplitude in plant sociology based on similarity of species content and its application to analyses of the vegetation on danish commons. *Biologiske Skrifter* **5**, 1–34 (1948) [5](#)
19. Thor, M., Petersen, J.B., Bentzen, L., Høyer, M., Muren, L.P.: Deformable image registration for contour propagation from CT to cone-beam CT scans in radiotherapy of prostate cancer. *Acta Oncologica* **50**(6), 918–925 (2011) [2](#)
20. Voyant, C., Biffi, K., Leschi, D., Briancon, J., Lantieri, C.: Dosimetric uncertainties related to the elasticity of bladder and rectal walls: Adenocarcinoma of the prostate. *Cancer/Radiothérapie* **15**(4), 270–278 (2011) [2](#)
21. Wasserthal, J., Breit, H.C., Meyer, M.T., Pradella, M., Hinck, D., Sauter, A.W., Heye, T., Boll, D.T., Cyriac, J., Yang, S., et al.: Totalsegmentator: robust segmentation of 104 anatomic structures in CT images. *Radiology: Artificial Intelligence* **5**(5), e230024 (2023) [4](#)

22. Zhu, J.Y., Park, T., Isola, P., Efros, A.A.: Unpaired image-to-image translation using cycle-consistent adversarial networks. In: Proceedings of the IEEE international conference on computer vision. pp. 2223–2232 (2017) [5](#)